


## Room-temperature magnetization reversal and magnetocaloric switching in Fe substituted GdMnO<sub>3</sub>

Arnab Pal,<sup>1,\*</sup> Manu Mohan,<sup>1</sup> Adyam Venimadhav,<sup>2</sup> and Pattukkannu Murugavel<sup>1,†</sup>

<sup>1</sup>*Department of Physics, Indian Institute of Technology Madras, Chennai 600036, India*

<sup>2</sup>*Cryogenic Engineering Centre, Indian Institute of Technology Kharagpur, Kharagpur 721302, India*

 (Received 7 November 2019; revised manuscript received 13 February 2020; accepted 27 March 2020; published 24 April 2020)

Room-temperature tunable bipolar magnetization switching and magnetically switchable magnetocaloric phenomena having numerous application potentials are reported in GdMn<sub>1-x</sub>Fe<sub>x</sub>O<sub>3</sub> ( $x = 0.55$  and  $0.60$ ) polycrystalline samples. Substitution of Fe in antiferromagnetic GdMnO<sub>3</sub> induces a first-order spin-reorientation transition ( $T_{SR}$ ), which along with antiferromagnetic ordering transition ( $T_N$ ) gives rise to anomalies in dielectric spectra, a signature of magnetodielectric effect. Temperature-dependent Raman spectra confirm the spin-phonon coupling which could be the origin of the magnetodielectric effect in the system. Notably, low-field magnetically tunable magnetization reversal is found to appear between  $T_{SR}$  and  $T_N$  in these compounds owing to the competition between single-ion magnetic anisotropy and antisymmetric Dzyaloshinsky-Moriya interaction. Additionally, the GdMn<sub>0.40</sub>Fe<sub>0.60</sub>O<sub>3</sub> sample reveals the coexistence of magnetically switchable conventional and inverse magnetocaloric effect at 250 and 310 K. The tailoring of these coexisting room-temperature magnetization reversal and magnetocaloric phenomena in a single-phase system suggests a route to design the material suitable for potential applications in electromagnetic and memory devices.

DOI: [10.1103/PhysRevMaterials.4.044407](https://doi.org/10.1103/PhysRevMaterials.4.044407)

### I. INTRODUCTION

Magnetodielectric materials are gaining importance due to the coupling between their dielectric and magnetic orders in same phase which is rare in nature [1–6]. Such systems can be either ferroelectric [7–10] or nonferroelectric [11–13], depending on their polar state. Even in nonferroelectric systems, the observed dielectric anomalies around magnetic transition temperatures can represent the magnetodielectric (MD) effect [14,15]. However, irrespective of their polar state, these systems are attractive to research both in the fundamental and application point of view [2,3,16,17]. On the other hand, observation of magnetization reversal (negative magnetization) without reversing the direction of magnetic field in a magnetic material is considered as a noteworthy phenomenon in magnetism [18–37]. This phenomenon was first predicted by Néel in certain ferrimagnetic materials such as spinel oxides having different magnetic sublattices [38]. The different temperature dependences in antiferromagnetic (AFM) exchange interactions between these sublattices yield a net zero magnetization at a characteristic temperature called compensation temperature below which a magnetization reversal occurs due to the domination of a particular sublattice [38,39]. Since then, this phenomenon was widely studied in various systems such as lithium chromium ferrite, orthovanadates,

garnets, molecular magnets, hexacyanides, and intermetallics with distinctly different origin in each system [18–23].

Recently, the magnetization reversal studies have been extended to rare-earth based oxides such as orthoferrites, orthochromites, manganites, and ruthenites with the mixed *A*- and *B*-site perovskite ( $ABO_3$ ) and double-perovskite ( $A_2BB'O_6$ ) structures [24–37]. It is primarily considered to be arisen from the competition between different magnetic interactions appearing at *A*- and *B*- sites. However, most of these systems show low compensation temperature, which restricts their application potential. Hence, designing the materials exhibiting magnetization reversal near room temperature is desirable to realize this phenomenon towards practical applications. YFe<sub>0.5</sub>Cr<sub>0.5</sub>O<sub>3</sub> and high-pressure synthesis of BiFe<sub>0.5</sub>Mn<sub>0.5</sub>O<sub>3</sub> are reported to serve this purpose to some extent with relatively high compensation temperatures at 248 and 208 K, respectively [31,40]. Although these works show the way of increasing compensation temperature, the observed values are far below room temperature. Additionally, designing the materials with high compensation temperature is gaining importance due to the fact that the conventional and inverse magnetocaloric effect (MCE) are reported near compensation temperature in few systems [21,31,33,37]. Henceforth, it is important to propose a material showing unusual room-temperature magnetization reversal and MCE properties for practical applications.

In this article, the single-phase perovskite GdMn<sub>1-x</sub>Fe<sub>x</sub>O<sub>3</sub> ( $x = 0.55$  and  $0.60$ ) system is chosen for the structural, dielectric, magnetic, and MCE studies. The two parent compounds of this system, namely GdMnO<sub>3</sub> and GdFeO<sub>3</sub> crystallize in orthorhombic structure with different magnetic transition

\*Present address: Materials Genome Institute, Shanghai University, Shanghai 200444, China.

†muruga@iitm.ac.in

temperatures [41,42]. While the former exhibits AFM ordering at low temperature ( $T_N \sim 40$  K) [43], the latter possesses spin-reorientation transition ( $T_{SR} \sim 4.2$  K) along with AFM ordering at high temperature ( $T_N \sim 661$  K) [42,44]. Consequently, the compounds are reported to show tunable magnetic ordering temperatures with composition and even exhibit the  $T_{SR}$  and  $T_N$  in the vicinity of room temperature for some intermediate compositions such as  $x = 0.55$  and  $0.60$  [45]. Since the competition between different magnetic interactions in this temperature region may result in magnetization reversal and switching of MCE around room temperature, these two compositions  $x = 0.55$  and  $0.60$  are selected for these studies. Interestingly, the compounds revealed magnetic-field switchable magnetization reversal phenomenon between the magnetic ordering temperatures  $T_{SR}$  and  $T_N$  around 300 K. Moreover, the compound also exhibits switching between conventional and inverse MCE near these magnetic transitions. The possible origin of negative magnetization along with the switchable MCE effect is elucidated in this work. Overall, the experimental findings presented in this work suggest the potential application of this material in fields such as magnetic memory, spintronics, etc.

## II. EXPERIMENTAL DETAILS

Polycrystalline  $\text{GdMn}_{1-x}\text{Fe}_x\text{O}_3$  ( $x = 0.55$  and  $0.60$ ) samples were prepared by the standard solid-state reaction method. The stoichiometric quantity of high-purity precursors  $\text{Gd}_2\text{O}_3$  (preheated at  $1000$  °C for 12 h),  $\text{Mn}_2\text{O}_3$ , and  $\text{Fe}_2\text{O}_3$  were mixed, ground in an agate mortar, and calcined at  $1000$  °C for 24 h under ambient condition. The obtained powders were ground again and recalcined at  $1100$ ,  $1200$ , and  $1300$  °C for 24 h each to achieve pure phase. The powder was then pressed into pellets followed by sintering at  $1400$  °C for 24 h to attain high density ( $>96\%$  of theoretical density). X-ray powder-diffraction (XRD) data were collected on the powder samples with a PANalytical x-ray diffractometer. Magnetic measurements were performed with a Quantum Design superconducting quantum interference device (SQUID) from 3 to 400 K under  $-7$  to  $7$  T fields. Dielectric measurements were carried out on the pellets, with silver coating on both surfaces as electrodes, using Novocontrol Alpha analyzer from 200 to 400 K. Temperature-dependent Raman experiments were carried out on the samples excited with  $632.8$ -nm wavelength in the backscattering geometry using HORIBA Jobin Yvon HR 800 UV Raman spectrometer. In addition, Quantum Design Physical Property Measurement System (PPMS) was incorporated to carry out the heat capacity measurement from 2 to 390 K using heat-pulse method.

## III. RESULTS AND DISCUSSION

The XRD patterns recorded on the samples along with the respective Rietveld refined data are plotted in Figs. 1(a) and 1(b) for  $x = 0.55$  and  $0.60$ , respectively. The pattern reveals phase-pure formation of the compound without any signature of impurity phases. The structural analysis on these compounds shows that they are crystallized in single-phase orthorhombic structure with  $Pnma$  space group. Al-

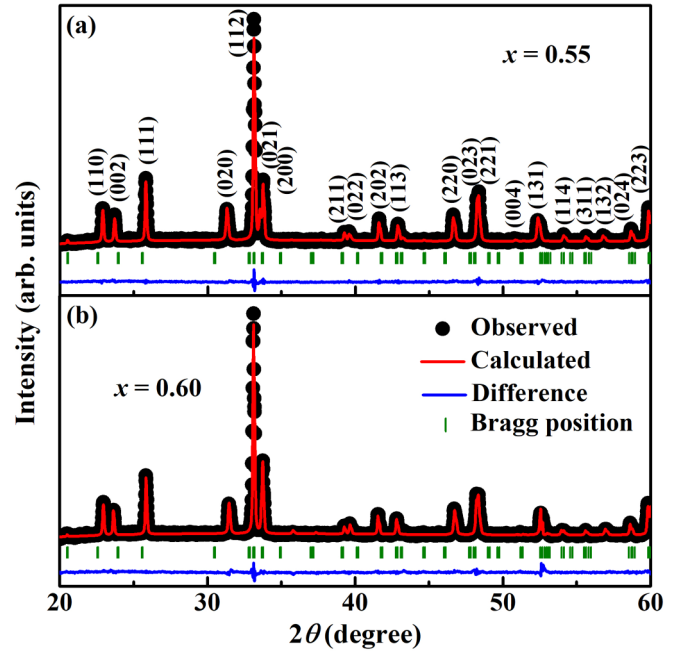


FIG. 1. XRD patterns recorded on (a)  $x = 0.55$  and (b)  $x = 0.60$  samples along with the Rietveld refined data.

though the reports on  $\text{GdMn}_{1-x}\text{Fe}_x\text{O}_3$  show linear variation in composition-dependent lattice parameter, the occupancy of Mn and Fe ions at same crystallographic site indicates the disorder arrangement of these two ions [45,46]. On the other hand, the presence of Fe ion makes the orbital ordering less stable in this mixed oxide system compared to pure  $\text{GdMnO}_3$  [45].

To explore the MD effect, dielectric measurements near magnetic transition temperatures are performed on  $\text{GdMn}_{1-x}\text{Fe}_x\text{O}_3$  ( $x = 0.55$  and  $0.60$ ) samples. Note that owing to high dielectric loss around room temperature [46], the anomaly in dielectric spectra near  $T_{SR}$  is not clearly visible for both samples. Hence, the temperature dependence of derivative of dielectric constant ( $d\epsilon_r'/dT$ ) measured at 5.3 MHz along with magnetization ( $M$ ) versus temperature ( $T$ ) curves near  $T_{SR}$  are plotted in Figs. 2(a) and 2(b) for  $x = 0.55$  and  $0.60$  samples, respectively. The  $T_{SR}$  of  $x = 0.55$  and  $0.60$  samples are indicated at 257 and 245 K in their respective  $M-T$  plots. A clear anomaly in dielectric plot near  $T_{SR}$  is observed for both the samples. This indicates a possible coupling between dielectric and magnetic orderings just below room temperature. The difference between the observed magnetic and dielectric transitions may appear due to the high dielectric loss that prevails in this system. Similarly, the respective derivative ( $d\epsilon_r'/dT$ ) plots near  $T_N$  are shown in Figs. 2(c) and 2(d) along with the  $M-T$  curves. The plots reveal dielectric anomalies near  $T_N$ , which are observed at 335 and 376 K for  $x = 0.55$  and  $0.60$  samples, respectively. The observed anomalies in  $d\epsilon_r'/dT$  plots near magnetic transitions can be attributed to the MD coupling in samples. The high dielectric loss in the sample [46] and subsequent instrumental limitation to perform the high-frequency ( $>1$  MHz) magnetocapacitance measurements restrict the quantification of the direct MD effect.

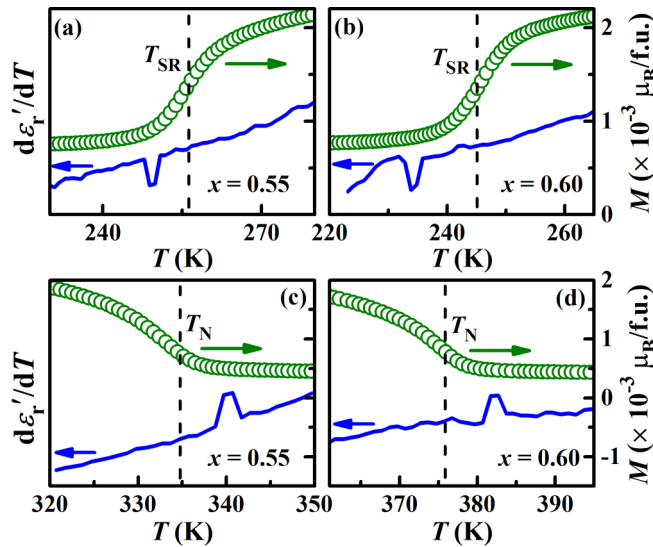


FIG. 2. Temperature dependence of derivative of dielectric constant and magnetization near  $T_{SR}$  for (a)  $x = 0.55$  and (b)  $x = 0.60$  samples. The respective plots near  $T_N$  for (c)  $x = 0.55$  and (d)  $x = 0.60$  samples.

It is known from the literature that as the temperature decreases the magnetic spin structure undergoes changes from paramagnetic to  $\Gamma_4$  and  $\Gamma_4$  to  $\Gamma_1$  across  $T_N$  and  $T_{SR}$ , respectively [45,46]. The corresponding spin arrangement initially changes its state from random to weak ferromagnetic (WFM) along the  $c$  axis and thereafter collinear AFM along the  $b$  axis. This may help to induce the MD coupling in the system. On the other hand, in the absence of ferroelectricity, the MD coupling may originate from some extrinsic factors like the Maxwell-Wagner effect and magnetoresistance in the system [11]. The Maxwell-Wagner effect can easily be ruled out as that must be uniform in a certain temperature range, while the possible MD effect is anticipated only near magnetic ordering temperatures. To verify the magnetoresistance contribution, the resistance of the sample is measured under zero field and 5-T field conditions. The resultant plots shown in Fig. S1, within the Supplemental Material [47], exhibit only a minor change in resistance under applied magnetic field in the desired temperature range and thereby eliminate significant contribution coming from the magnetoresistance effect if any in the sample. Therefore, the possible origin of the expected MD effect in this system could come from the spin rearrangement around magnetic ordering temperatures.

To understand the long-range or short-range nature of magnetic transitions at  $T_{SR}$  and  $T_N$ , heat capacity measurement is carried out in warming cycle from 200 to 390 K on  $x = 0.60$  sample using heat-pulse method and the corresponding thermodynamic data are presented in Fig. 3. The data include both lattice and magnetic contributions to heat capacity. The figure indicates an anomaly around  $T_{SR}$  and  $T_N$ , suggesting the long-range ordering of both magnetic transitions [48,49]. Additionally, the heat capacity of the same sample from 2 to 30 K shown in the inset of Fig. 3 exhibits an anomaly at 2.7 K corresponding to the AFM ordering of rare-earth Gd ion ( $T_{Gd}$ ) in consistent with the reported  $T_{Gd}$  for pure  $GdMnO_3$  [41] and  $GdFeO_3$  [42,44].

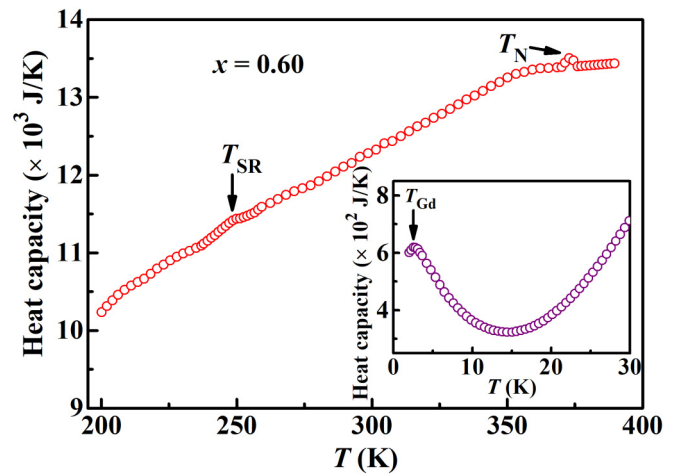


FIG. 3. Heat capacity versus temperature plot for  $x = 0.60$  sample from 200 to 390 K. Inset exhibits similar plot at lower temperature.

To probe these transitions further, Raman spectra are recorded in the temperature range covering  $T_{SR}$  and  $T_N$  for  $x = 0.55$  and  $0.60$  samples and the resultant plots are shown in Figs. 4(a) and 4(b), respectively. The intensity of spectra gradually decreases with increase in temperature for both the samples. Various phonon modes corresponding to different vibrational symmetries are assigned in Fig. 4(b). The lattice dynamical calculations and group-theoretical analysis predict that overall there are 24 Raman active modes ( $7A_g + 5B_{1g} + 7B_{2g} + 5B_{3g}$ ) in orthorhombic perovskite system [50]. Among these,  $A_g$  modes are assigned to  $BO_6$  octahedra bending or rotation and O2 antistretching, while  $B_{2g}$  and  $B_{3g}$  represent in-plane and out-of-plane properties, respectively [51]. Prior to temperature-dependence studies of  $B_{2g}$  and  $B_{3g}$  modes, the intense Raman peak centered around  $625\text{ cm}^{-1}$  measured at 208 K is deconvoluted and the prominent phonon modes at  $622$  and  $646\text{ cm}^{-1}$  corresponding to  $B_{2g}$  and  $B_{3g}$  symmetries, respectively, are shown in Fig. 4(c).  $B_{2g}$  is attributed to in-plane O2 stretching while  $B_{3g}$  is related to out-of-plane O2 stretching of Jahn-Teller (J-T) distorted  $BO_6$  octahedra ( $B = Mn/Fe$ ) [52].

To analyze it further, the frequencies of  $B_{2g}$  and  $B_{3g}$  modes are extracted at different temperatures and plotted as a function of temperature in Figs. 5(a) and 5(b) for  $x = 0.55$  and  $0.60$ , respectively. In general, in the absence of spin-phonon coupling, temperature dependence of phonon frequency defines the anharmonic phonon-phonon scattering. In this case, the frequencies of both  $B_{2g}$  and  $B_{3g}$  modes decrease with increase in temperature. Also, the compounds show an abnormal temperature-dependence behavior of both  $B_{2g}$  and  $B_{3g}$  modes with a significant deviation at  $T_N$  and  $T_{SR}$ . Since the system evolves from one type of spin structure to another type across these magnetic transitions, this anomalous behavior around  $T_N$  and  $T_{SR}$  indicates the correlation between presence of spin-phonon coupling caused by the phonon modulation of spin-exchange integral [52,53]. These results suggest that the spin-phonon coupling is associated with the MD effect. Since  $B_{2g}$  and  $B_{3g}$  modes are related to the J-T distortion, anomalies in these modes observed at magnetic transitions

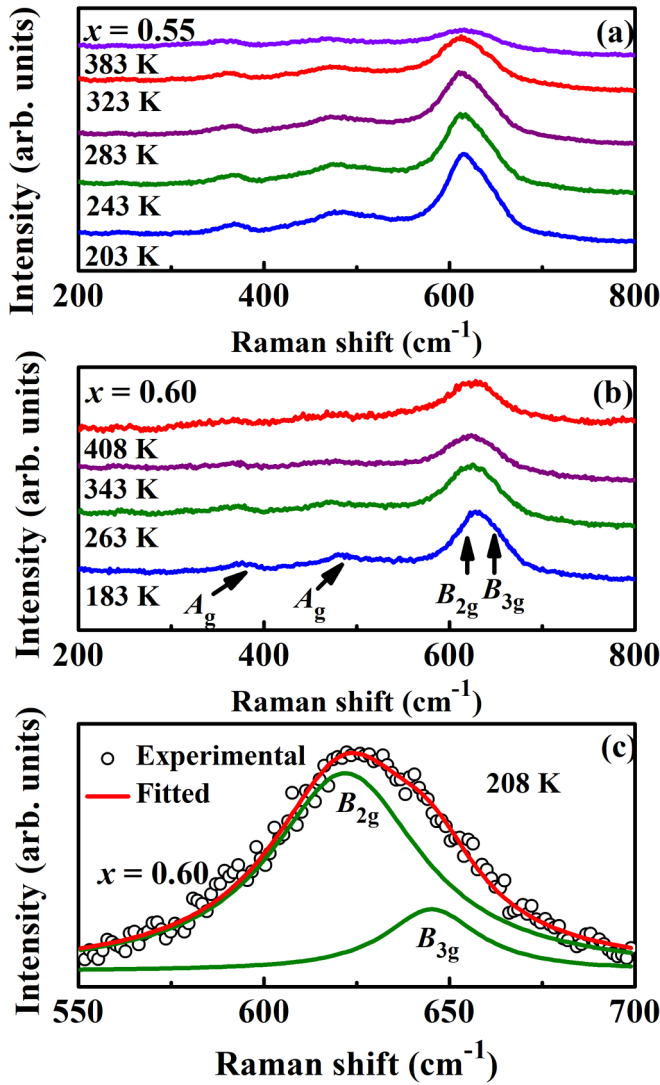


FIG. 4. Temperature-dependent Raman spectra for (a)  $x = 0.55$  and (b)  $x = 0.60$ . (c) The deconvoluted peak centered around  $625 \text{ cm}^{-1}$  into  $B_{2g}$  and  $B_{3g}$  phonon modes.

strongly suggest the specific role of J-T effect on the magnetic orderings in  $\text{GdMn}_{1-x}\text{Fe}_x\text{O}_3$  samples.

Temperature-dependent dc magnetization measurements are carried out at various magnetic fields (5 to 1000 Oe) under zero-field-cooled (ZFC), field-cooled cooling (FCC), and field-cooled warming (FCW) modes. The results are plotted for  $x = 0.55$  and 0.60 compounds in Figs. 6(a) and 6(b), respectively. The plots reveal some fascinating and unusual magnetic behaviors. The magnetization curves in Fig. 6(a) for  $x = 0.55$  show the onset of AFM ordering at 335 K ( $T_N$ ) which is attributed to the one to one ordering between  $\text{Fe}^{3+}$  and  $\text{Mn}^{3+}$  ions. On further cooling the sample in FCC and FCW modes, magnetization value increases with a maximum value at 296 K and thereafter decreases until reaching the magnetic ordering at 257 K ( $T_{SR}$ ). Below  $T_{SR}$ , the magnetization value is maintained to be low in magnitude owing to change in spin structure from  $\Gamma_4$  to  $\Gamma_1$ . Interestingly, the data recorded in ZFC mode show negative magnetization features between  $T_N$  and  $T_{SR}$ . This phenomenon is known as temperature-

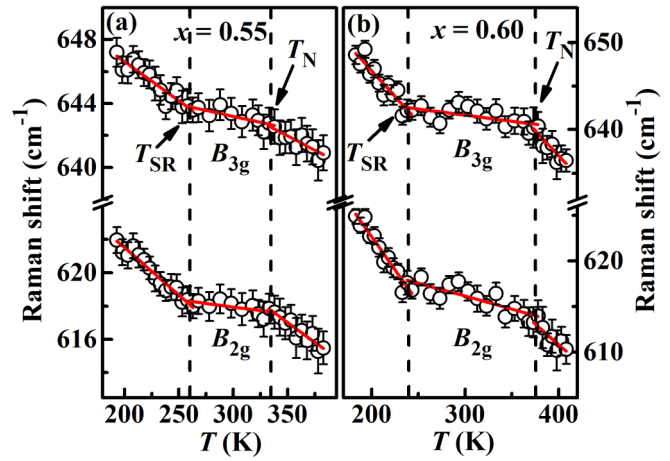


FIG. 5. Temperature dependence of frequency of  $B_{2g}$  and  $B_{3g}$  phonon modes across the  $T_{SR}$  and  $T_N$  for (a)  $x = 0.55$  and (b)  $x = 0.60$  compositions. Circles indicate the experimental points and solid lines are guide to the eye to demonstrate the deviations near magnetic ordering temperatures.

induced magnetization reversal and it shows that the direction of magnetization is opposite to the applied magnetic field. Most noteworthy observation is that the temperatures near  $T_N$  and  $T_{SR}$  serve as compensation temperature at which

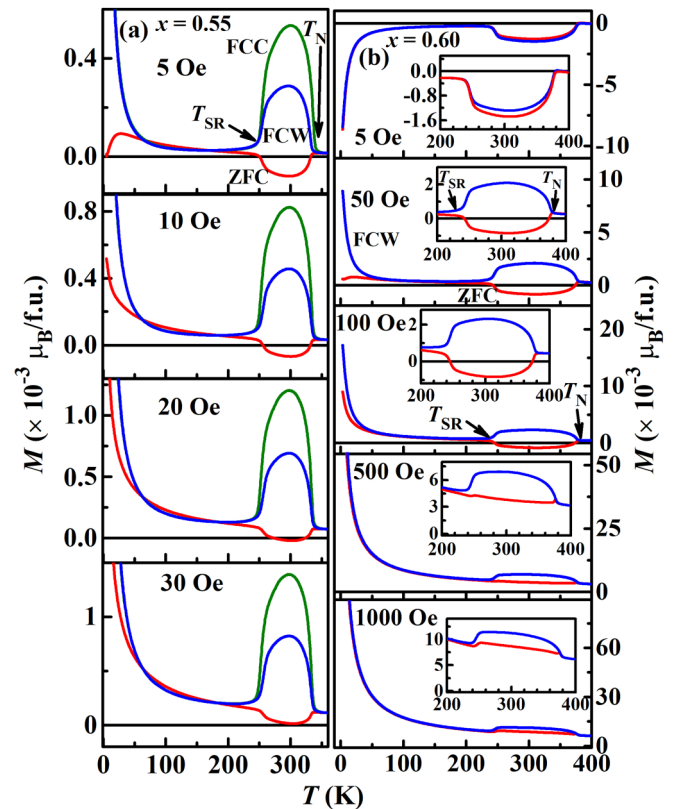


FIG. 6. Temperature dependence of magnetization ( $M-T$ ) plots at various magnetic fields shown for (a)  $x = 0.55$  in ZFC, FCC, and FCW modes and (b)  $x = 0.60$  in ZFC and FCW modes. The insets show the enlarged version of the respective  $M-T$  curves across  $T_{SR}$  and  $T_N$ .

magnetization will be zero, and sign of the magnetization can be switched between negative and positive value near these magnetic transitions by change in temperature. It is also worth to mention that as we increase the magnetic field, ZFC magnetization undergoes switching from negative to positive value above 20 Oe for  $x = 0.55$  sample.

Notably, the negative ZFC magnetization is sustained between  $T_{SR}$  (245 K) and  $T_N$  (376 K) at a field up to 100 Oe for  $x = 0.60$  sample [see the insets in Fig. 6(b) showing the enlarged version of the respective plots across  $T_{SR}$  and  $T_N$ ]. Furthermore, the data recorded in FCW mode also show the magnetization reversal but at a field  $\leq 5$  Oe. As the field is increased from 5 to 500 Oe, the negative magnetization seen in ZFC mode gradually decreases in magnitude and switches to a positive value. Moreover, magnetization plots near Gd-ordering temperature show negative values at 5 Oe field for both ZFC and FCW data, and switched to positive values at higher fields. Overall, the magnitude of the negative magnetization for  $x = 0.60$  sample is an order of degree higher than the value shown by  $x = 0.55$  sample.

To ascertain the intrinsic nature of the negative magnetization data, it is essential to rule out the possible extrinsic origins. One such extrinsic origin could be the effect of trapped field on the magnetization data as reported earlier in few samples such as  $YMn_{0.5}Cr_{0.5}O_3$  and  $CoCr_2O_4$  [32,54]. The trapped field is the small remnant field remaining in the magnetic measurement instrument owing to the trapped magnetic flux inside the superconducting material. The negative trapped field (NTF) appears in the instrument when the field is reduced to zero from a high positive field and the positive trapped field (PTF) appears when the field is reduced to zero from the initial high negative field [54]. In the present work, the NTF and PTF are generated by applying the maximum field of  $\pm 1$  T. Then, the temperature-dependent ZFC magnetization measurement is repeated for  $x = 0.55$  sample under both PTF and NTF. The magnetization data shown in Fig. S2, within the Supplemental Material [47], exhibit almost equivalent negative magnetization phenomenon measured under both fields and they are similar to the one observed for 5 Oe ZFC data for  $x = 0.60$ . The similarity comes from the fact that 5 Oe field can change the direction of the magnetization in  $x = 0.55$ , while it is not sufficient to switch the negative magnetization observed in  $x = 0.60$  sample. This observation is opposite to the reported results where the PTF and NTF effects are demonstrated to exhibit magnetization data which are mirror image to each other [32,54]. This measurement excludes the extrinsic contributions coming from the trapped fields and confirms that the observed negative magnetization phenomenon in  $GdMn_{1-x}Fe_xO_3$  ( $x = 0.55$  and 0.60) samples is indeed intrinsic in origin.

Additionally, extreme care has been taken to avoid any diamagnetic contributions from the sample holder and measurement geometry. To be clear about the sample signal, the magnetic measurements are carried out using a quartz holder which has a background signal of  $10^{-7}$  emu (electromagnetic unit). Note that the sample signal is  $\sim 10^{-5}$  emu for 30 mg at room temperature and it changes by an order of magnitude down to low temperature while the SQUID signal from the quartz holder remains the same. This further eliminates the possibilities of the diamagnetic contributions if any from the

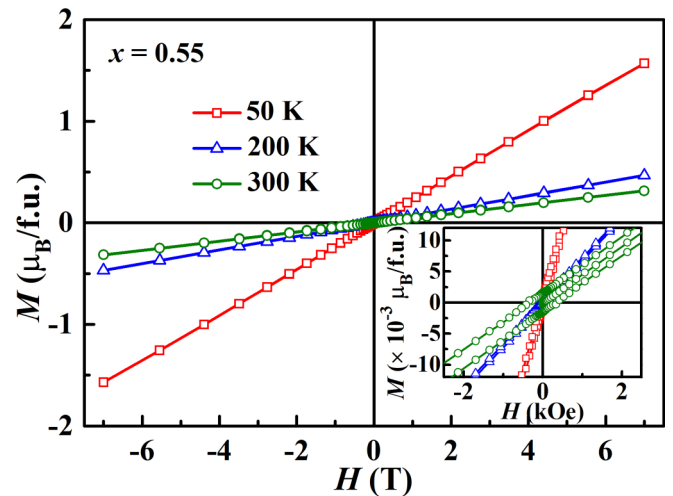


FIG. 7. Magnetization versus magnetic field ( $M$ - $H$ ) plots at 50, 200, and 300 K for  $x = 0.55$  sample. Inset shows enlarged version of the respective plots at lower magnetic-field range.

sample holder to the observed magnetic behavior. Also, if this effect is an extrinsic or external artifact then the magnetization would have been negative in the whole temperature range below  $T_N$ . However, we have seen the negative magnetization only between  $T_{SR}$  and  $T_N$ . In addition, the artifact will not give an order of magnitude difference in magnetization between  $x = 0.55$  and 0.60 samples. These facts indicate that the magnetization reversal features are indeed intrinsic in nature.

To analyze it further, it is necessary to confirm the ground state of these compounds from isothermal magnetization ( $M$ - $H$ ) data. As a representative example, Fig. 7 shows the  $M$ - $H$  plots of  $x = 0.55$  composition from  $-7$  to  $7$  T measured at 50, 200, and 300 K. Ordered arrangement between  $Fe^{3+}$  and  $Mn^{3+}$  ions at  $B$  site would have resulted in ferromagnetic (FM) features as reported earlier in several double-perovskite compounds like  $La_2NiMnO_6$  [4],  $La_2CoMnO_6$  [13],  $Er_2CoMnO_6$  [36], and  $Gd_2NiMnO_6$  [55] where  $B$ -site ions are ordered in rocksalt configuration. However, the plots show that overall magnetic interaction is AFM at all temperatures. This indicates that the  $Mn^{3+}$  and  $Fe^{3+}$  ions are randomly distributed without any specific ordering at  $B$  site. To further verify the magnetic states at different temperatures, the enlarged version of the  $M$ - $H$  plots at low fields is shown in the inset of Fig. 7. While a clear loop opening is observed at 300 K indicating the WFM ordering, the absence of it in the plots measured at lower temperatures (200 and 50 K) displays collinear AFM ordering. These observations support the proposed magnetic structural change from  $\Gamma_4$  (WFM) to  $\Gamma_1$  (collinear AFM) across the  $T_{SR}$  (257 K for  $x = 0.55$  sample) as discussed earlier.

In the present compounds, the random distribution of magnetic ions at  $B$  site rules out the Néel model involving three different magnetic sublattices [38,39]. On the other hand, the observed negative magnetization in these compounds is confined in the WFM region while collinear AFM region ( $< T_{SR}$ ) shows positive magnetization. In general, the appearance of WFM character is determined by either of the two mechanisms, namely single-ion magnetic anisotropy

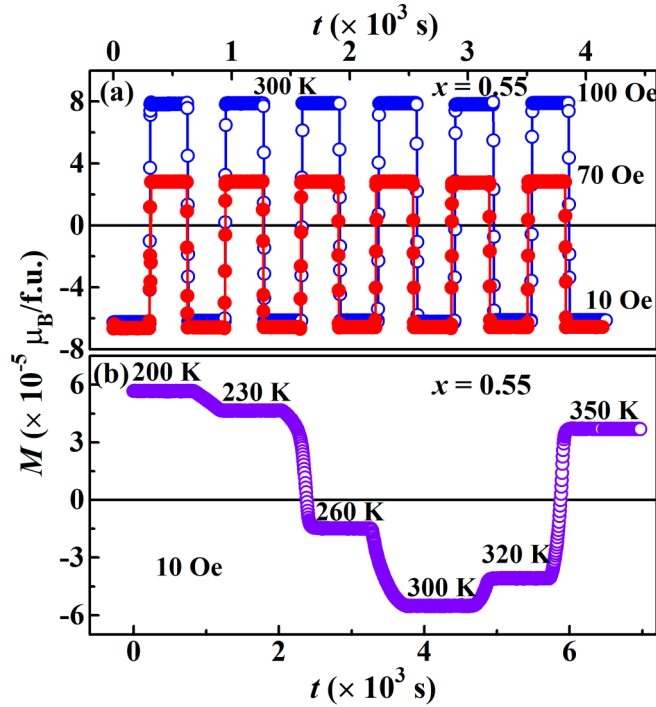


FIG. 8. Time dependence of magnetization plots (a) at 300 K for different magnetic fields and (b) at 10-Oe field for various temperatures for  $x = 0.55$  sample.

(SIMA) and antisymmetric Dzyaloshinsky-Moriya (DM) interaction [56]. The net moments produced by these mechanisms may be added up in some cases, while in the mixed  $B$ -site compounds the different temperature dependences of these moments can be oriented in different directions which results in the presence of negative magnetization at low-applied fields [31,40]. In this instance, one of the end members,  $\text{GdFeO}_3$ , is a canted antiferromagnet owing to the DM interaction [44]. Substitution of Mn ion at the Fe site enhances the  $T_{\text{SR}}$  and decreases the  $T_{\text{N}}$  due to the increase of Mn-SIMA in the system and brings out the necessary competition between Mn-SIMA and DM interaction [45]. It is believed that the net moments produced by these factors are oriented in opposite direction and the resultant magnetization is in antiparallel direction to the external field at low-field values. This demonstrates the maximum room-temperature negative magnetization in  $x = 0.60$  sample as it may prominently favor the competition between Mn-SIMA and DM interaction. However, by applying a large magnetic field, it is possible to overcome the average magnetic anisotropy and as a consequence, the switching of resultant magnetic moment parallel to the field direction results in the appearance of positive magnetization. This isothermal spin-reversal phenomenon can be further confirmed by a tunable bipolar switching of magnetization at a given temperature in between  $T_{\text{SR}}$  and  $T_{\text{N}}$ .

Figure 8(a) demonstrates ZFC magnetization data switching between negative and positive values for  $x = 0.55$  composition, when the magnetization is recorded for selected duration of time under 10, 70, and 100 Oe fields at 300 K. In this measurement, initially, the sample is cooled from a high temperature ( $>T_{\text{N}}$ ) to 300 K under zero magnetic field

and then the field is increased to 10 Oe and kept constant for certain duration of time. Further, the field is increased to 100 Oe to switch the magnetization to an equivalent positive value and maintain it for the fixed time duration. The process is continued for several cycles to verify the reproducibility of the switching behavior. The observed data plotted in Fig. 8(a) show a perfect field-induced magnetization reversal phenomenon at 300 K. The process is repeated for another combination of fields (70 and 10 Oe) at the same temperature. These data confirm that the negative magnetization as observed from the figure is stable under different sets of fields. It is inferred from Fig. 8(a) that the magnetization can be altered between a positive and negative value by just tuning the magnitude of the applied magnetic field along the positive direction. It is clearly advantageous over FM system, where the direction of the stable polar states is independent of the magnitude of field strength. Although the similar demonstration of spin reversal is established in other perovskite compounds like  $\text{BiFe}_{0.5}\text{Mn}_{0.5}\text{O}_3$  [40] and  $\text{YFe}_{0.5}\text{Cr}_{0.5}\text{O}_3$  [31], they are at temperatures far below 300 K. The present compound displays room-temperature ( $\sim 300$  K) phenomenon which may be beneficial for potential applications in magnetic data storage and nonvolatile magnetic memory devices.

In order to verify the stability of the negative magnetization at a certain temperature, the time-dependent magnetization measurement for  $x = 0.55$  sample is repeated for various temperatures under 10-Oe field and the corresponding data are plotted in Fig. 8(b). Here, the sample is cooled from a temperature above  $T_{\text{N}}$  to 200 K under zero magnetic field and then the magnetization is recorded at 200 K under 10-Oe magnetic field for a fixed duration of time. The process is repeated for other temperatures under the same field. As expected, the magnetization data show negative values when recorded at temperatures between  $T_{\text{SR}}$  and  $T_{\text{N}}$  (260, 300, and 320 K) with profound effect at 300 K and switched to positive value at 230 K (below  $T_{\text{SR}}$ ) and 350 K (above  $T_{\text{N}}$ ) which are consistent with the  $M$ - $T$  data shown in Fig. 6(a). The time-dependent magnetic measurement illustrates the stability of the magnetization values at all temperatures.

Significantly, the negative and positive slope variations of magnetization with decreasing temperature can yield conventional and inverse MCE, respectively [21,31,37]. Since the present compounds show both positive and negative magnetization as a function of temperature near  $T_{\text{SR}}$  and  $T_{\text{N}}$ , it is expected to show both MCEs in these systems. It is known that the temperature dependence of magnetic entropy change ( $-\Delta S_{\text{M}}$ ) with the application of magnetic field results in the appearance of MCE in the system. To extract the thermal variation of  $-\Delta S_{\text{M}}$  for  $x = 0.60$  composition the temperature-dependent ZFC magnetization data [from Fig. 6(b)] are used in the Maxwell equation [21,31,37],

$$|\Delta S_{\text{M}}| = \sum \left[ \left( \frac{\partial M}{\partial T} \right)_{H_i} + \left( \frac{\partial M}{\partial T} \right)_{H_{i+1}} \right] \left( \frac{\Delta H_i}{2} \right), \quad (1)$$

where  $\left( \frac{\partial M}{\partial T} \right)_{H_i}$  and  $\left( \frac{\partial M}{\partial T} \right)_{H_{i+1}}$  are the first derivatives of ZFC magnetization at  $H_i$  and  $H_{i+1}$  magnetic fields, respectively. The temperature dependence of  $-\Delta S_{\text{M}}$  is plotted in Fig. 9 for  $x = 0.60$  sample for various magnetic fields and the

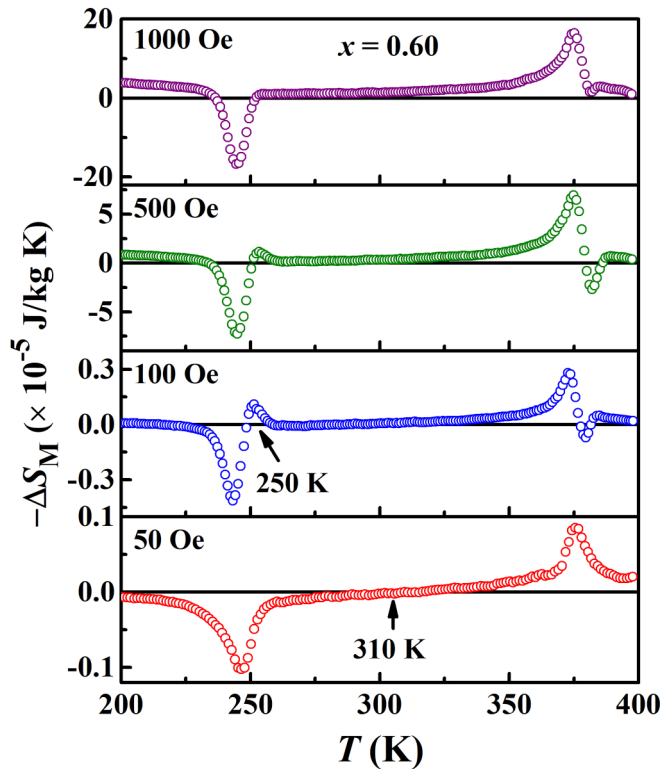


FIG. 9. Magnetic entropy change ( $-\Delta S_M$ ) in  $x = 0.60$  sample as a function of temperature for different magnetic fields.

polarity reversal of  $-\Delta S_M$ , observed from this plot, is a direct consequence of the change in sign of  $\Delta M/\Delta T$  [31,37]. The  $-\Delta S_M$  value is increasing with the magnetic field from 50 to 1000 Oe in accordance with the usual behavior of MCE. The interesting feature is revealed at 50-Oe field. Here, by decreasing the temperature from 400 K,  $-\Delta S_M$  reaches a maximum at 376 K ( $T_N$ ) and decreases thereafter. Remarkably, on further cooling the sample, the  $-\Delta S_M$  reaches zero value at 310 K and changes its sign to show the inverse MCE which becomes maximum at 245 K ( $T_{SR}$ ). The similar feature is observed for 100-Oe field with  $-\Delta S_M = 0$  at 250 K. This unusual coexistence of conventional and inverse MCEs with switching at a particular temperature makes this compound a promising material for a constant-temperature bath appli-

cation as proposed by Yusuf *et al.* [21]. As an example, if the material is used as a working medium at 50-Oe field and at  $T > 310$  K, the positive  $-\Delta S_M$  will decrease the temperature and keep it constant at 310 K while at  $T < 310$  K, the negative  $-\Delta S_M$  will increase the temperature until it reaches 310 K. Hence, any temperature fluctuation near 310 K can be balanced by these two complementary MCEs. The observed remarkable feature revealed by this compound has potential use for constant-temperature baths (at 310 and 250 K) by changing the applied magnetic field from 50 to 100 Oe.

#### IV. CONCLUSIONS

In summary, we have presented a correlation between dielectric and magnetic orderings with detailed study on unusual magnetic properties of orthorhombic perovskite  $\text{GdMn}_{1-x}\text{Fe}_x\text{O}_3$  ( $x = 0.55$  and  $0.60$ ) compounds. Both spin-reorientation and antiferromagnetic transitions are displayed by magnetic and heat capacity measurements. A clear anomaly observed in dielectric spectra near the magnetic transitions may indicate a possible room-temperature magnetodielectric effect which is originated from the spin-phonon coupling as revealed from Raman spectra. Interestingly, this compound exhibits room-temperature magnetization reversal at low magnetic fields. This unusual phenomenon arising from the competition between single-ion magnetic anisotropy and Dzyaloshinsky-Moriya interaction results in a tunable bipolar switching of magnetization along with low-field conventional and inverse magnetocaloric effect at room temperature. Although microscopic understanding is necessary to apply this material for practical purpose, current work provides a possible way to design its use in nonvolatile memories and magnetic heating based constant-temperature bath. Overall, the noteworthy room-temperature multifunctional properties make this system significant for fundamental studies with great promise for suitable applications.

#### ACKNOWLEDGMENTS

The authors acknowledge Dr. C. Dhana Sekhar for his help in doing some magnetic measurements. The DST-FIST funding (Project No. SR/FST/PSII-038/2016) for the Department of Physics PPMS facility is acknowledged.

- [1] N. A. Spaldin and M. Fiebig, *Science* **309**, 391 (2005).
- [2] M. Fiebig, *J. Phys. D: Appl. Phys.* **38**, R123 (2005).
- [3] W. Eerenstein, N. D. Mathur, and J. F. Scott, *Nature (London)* **442**, 759 (2006).
- [4] N. S. Rogado, J. Li, A. W. Sleight, and M. A. Subramanian, *Adv. Mater.* **17**, 2225 (2005).
- [5] T. Kimura, S. Kawamoto, I. Yamada, M. Azuma, M. Takano, and Y. Tokura, *Phys. Rev. B* **67**, 180401(R) (2003).
- [6] J. Magesh, P. Murugavel, R. V. K. Mangalam, K. Singh, C. Simon, and W. Prellier, *J. Appl. Phys.* **118**, 074102 (2015).
- [7] T. Kimura, G. Lawes, T. Goto, Y. Tokura, and A. P. Ramirez, *Phys. Rev. B* **71**, 224425 (2005).
- [8] S. Goswami, D. Bhattacharya, P. Choudhury, B. Ouladdiaf, and T. Chatterji, *Appl. Phys. Lett.* **99**, 073106 (2011).
- [9] R. C. Rai, J. Cao, J. L. Musfeldt, S. B. Kim, S.-W. Cheong, and X. Wei, *Phys. Rev. B* **75**, 184414 (2007).
- [10] A. Pal, W. Prellier, and P. Murugavel, *J. Phys.: Condens. Matter* **30**, 125801 (2018).
- [11] G. Catalan, *Appl. Phys. Lett.* **88**, 102902 (2006).
- [12] G. Lawes, T. Kimura, C. M. Varma, M. A. Subramanian, N. Rogado, R. J. Cava, and A. P. Ramirez, *Prog. Solid State Chem.* **37**, 40 (2009).
- [13] A. Venimadhav, D. Chandrasekhar, and J. K. Murthy, *Appl. Nanosci.* **3**, 25 (2013).

- [14] T. Kimura, S. Ishihara, H. Shintani, T. Arima, K. T. Takahashi, K. Ishizaka, and Y. Tokura, *Phys. Rev. B* **68**, 060403(R) (2003).
- [15] F. Hong, Z. Cheng, and X. Wang, *J. Appl. Phys.* **112**, 013920 (2012).
- [16] F. Schrettle, P. Lunkenheimer, J. Hemberger, V. Y. Ivanov, A. A. Mukhin, A. M. Balbashov, and A. Loidl, *Phys. Rev. Lett.* **102**, 207208 (2009).
- [17] C.-H. Yang, T. Y. Koo, and Y. H. Jeong, *Solid State Commun.* **134**, 299 (2005).
- [18] E. W. Gorter and J. A. Schulkes, *Phys. Rev.* **90**, 487 (1953).
- [19] Y. Ren, T. T. M. Palstra, D. I. Khomskii, E. Pellegrin, A. A. Nugroho, A. A. Menovsky, and G. A. Sawatzky, *Nature (London)* **396**, 441 (1998).
- [20] R. Pauthenet, *J. Appl. Phys.* **29**, 253 (1958).
- [21] S. M. Yusuf, A. Kumar, and J. V. Yakhmi, *Appl. Phys. Lett.* **95**, 182506 (2009).
- [22] S.-I. Ohkoshi, T. Hozumi, and K. Hashimoto, *Phys. Rev. B* **64**, 132404 (2001).
- [23] B. Andrzejewski, A. Kowalczyk, J. E. Frąckowiak, T. Tolinski, A. Szlaferek, S. Pal, and C. Simon, *Phys. Status Solidi B* **243**, 295 (2006).
- [24] K. Yoshii, *J. Solid State Chem.* **159**, 204 (2001).
- [25] Y. Su, J. Zhang, Z. Feng, L. Li, B. Li, Y. Zhou, Z. Chen, and S. Cao, *J. Appl. Phys.* **108**, 013905 (2010).
- [26] S. Huang, G. Zerihun, Z. Tian, S. Yuan, G. Gong, C. Yin, and L. Wang, *Ceram. Int.* **40**, 13937 (2014).
- [27] K. Yoshii, A. Nakamura, Y. Ishii, and Y. Morii, *J. Solid State Chem.* **162**, 84 (2001).
- [28] V. A. Khomchenko, I. O. Troyanchuk, R. Szymczak, and H. Szymczak, *J. Mater. Sci.* **43**, 5662 (2008).
- [29] Y. Ma, M. Guilloux-Viry, P. Barahona, O. Pena, and C. Moure, *Appl. Phys. Lett.* **86**, 062506 (2005).
- [30] H. Nhalil, H. S. Nair, R. Sanathkumar, A. M. Strydom, and S. Elizabeth, *J. Appl. Phys.* **117**, 173904 (2015).
- [31] J. Mao, Y. Sui, X. Zhang, Y. Su, X. Wang, Z. Liu, Y. Wang, R. Zhu, Y. Wang, W. Liu, and J. Tang, *Appl. Phys. Lett.* **98**, 192510 (2011).
- [32] X. Xie, H. Che, H. Wang, G. Lin, and H. Zhu, *Inorg. Chem.* **57**, 175 (2018).
- [33] P. Mandal, C. R. Serrao, E. Suard, V. Caignaert, B. Raveau, A. Sundaresan, and C. N. R. Rao, *J. Solid State Chem.* **197**, 408 (2013).
- [34] P. S. R. Murthy, K. R. Priolkar, P. A. Bhoje, A. Das, P. R. Sarode, and A. K. Nigam, *J. Magn. Magn. Mater.* **322**, 3704 (2010).
- [35] R. P. Singh and C. V. Tomy, *J. Phys.: Condens. Matter* **20**, 235209 (2008).
- [36] A. Banerjee, J. Sannigrahi, S. Giri, and S. Majumdar, *Phys. Rev. B* **98**, 104414 (2018).
- [37] J. K. Murthy and A. Venimadhav, *Physica B* **448**, 162 (2014).
- [38] L. Neel, *Ann. Phys.* **12**, 137 (1948).
- [39] O. Kahn, *Nature (London)* **399**, 21 (1999).
- [40] P. Mandal, A. Sundaresan, C. N. R. Rao, A. Iyo, P. M. Shirage, Y. Tanaka, C. Simon, V. Pralong, O. I. Lebedev, V. Caignaert, and B. Raveau, *Phys. Rev. B* **82**, 100416(R) (2010).
- [41] A. Pal, C. Dhanasekhar, A. Venimadhav, W. Prellier, and P. Murugavel, *J. Appl. Phys.* **123**, 014102 (2018).
- [42] G. W. Durbin, C. E. Jhonson, and M. F. Thomas, *J. Phys. C: Solid State Phys.* **10**, 1975 (1977).
- [43] L. Lin, L. Li, Z. B. Yan, Y. M. Tao, S. Dong, and J.-M. Liu, *Appl. Phys. A* **112**, 947 (2013).
- [44] Y. Tokunaga, N. Furukawa, H. Sakai, Y. Taguchi, T.-H. Arima, and Y. Tokura, *Nat. Mater.* **8**, 558 (2009).
- [45] A. Pal, C. Dhanasekhar, A. Venimadhav, and P. Murugavel, *J. Phys.: Condens. Matter* **29**, 405803 (2017).
- [46] A. Pal and P. Murugavel, *Physica B: Condens. Matter* **555**, 99 (2019).
- [47] See Supplemental Material at <http://link.aps.org/supplemental/10.1103/PhysRevMaterials.4.044407> for the magnetoresistance measurement of  $x = 0.60$  sample at 0- and 5-T fields where it exhibits a minor change in resistance under applied magnetic field near magnetic transition temperatures; temperature dependence of magnetization ( $M-T$ ) plots under NTF and PTF for  $x = 0.55$  sample which show almost equivalent negative magnetization phenomenon measured under both the fields.
- [48] G. Lawes, B. Melot, K. Page, C. Ederer, M. A. Hayward, T. Proffen, and R. Seshadri, *Phys. Rev. B* **74**, 024413 (2006).
- [49] R. Fichtl, V. Tsurkan, P. Lunkenheimer, J. Hemberger, V. Fritsch, H.-A. Krug von Nidda, E.-W. Scheidt, and A. Loidl, *Phys. Rev. Lett.* **94**, 027601 (2005).
- [50] M. N. Iliev, M. V. Abrashev, H.-G. Lee, V. N. Popov, Y. Y. Sun, C. Thomsen, R. L. Meng, and C. W. Chu, *Phys. Rev. B* **57**, 2872 (1998).
- [51] M. N. Iliev, B. Lorenz, A. P. Litvinchuk, Y.-Q. Wang, Y. Y. Sun, and C. W. Chu, *J. Phys.: Condens. Matter* **17**, 3333 (2005).
- [52] P. Mandal, V. S. Bhadrani, Y. Sundarayya, C. Narayana, A. Sundaresan, and C. N. R. Rao, *Phys. Rev. Lett.* **107**, 137202 (2011).
- [53] E. Granado, A. Garcia, J. A. Sanjurjo, C. Rettori, I. Torriani, F. Prado, R. D. Sanchez, A. Caneiro, and S. B. Oseroff, *Phys. Rev. B* **60**, 11879 (1999).
- [54] N. Kumar and A. Sundaresan, *Solid State Commun.* **150**, 1162 (2010).
- [55] J. K. Murthy, K. D. Chandrasekhar, S. Mahana, D. Topwal, and A. Venimadhav, *J. Phys. D: Appl. Phys.* **48**, 355001 (2015).
- [56] I. Dzyaloshinsky, *J. Phys. Chem. Solids* **4**, 241 (1958).